IOP Publishing Journal of Physics: Condensed Matter
J. Phys.: Condens. Matter **32** (2020) 274001 (14pp) https://doi.org/10.1088/1361-648X/ab7d66

Experimental observation of density fluctuations in liquid metals associated with liquid–liquid, liquid–gas and metal–nonmetal transitions

Y Kajihara[1,4], M Inui[1], K Ohara[2] and K Matsuda[3]

[1] Graduate School of Integrated Arts and Sciences, Hiroshima University, Higashi-Hiroshima, 739-8521, Japan
[2] JASRI/SPring-8, Sayo-cho, Sayo-gun, Hyogo, 679-5198, Japan
[3] Graduate School of Science, Kyoto University, Kyoto, 606-8502, Japan

E-mail: kajihara@hiroshima-u.ac.jp

Received 24 September 2019, revised 28 February 2020
Accepted for publication 6 March 2020
Published 7 April 2020

Abstract

We have developed a special technique and succeeded to carry out small-angle x-ray scattering measurements for some liquid metal systems. The purpose is to investigate effects of transitions such as liquid–liquid (LLT), liquid–gas (LGT) and metal–nonmetal (MNMT) transitions on mesoscopic density fluctuations in liquids. In liquid Te systems (Se–Te and Ge–Te mixtures), which show continuous LLT accompanying MNMT, parameters of density fluctuations show maxima almost in the middle of the transition, both in strength and spatial size. This work (and Kajihara *et al* 2012 *Phys. Rev.* **B86** 214202) was the first direct observation that density fluctuations exhibit maximum corresponding to LLT. However in this study, we could not clearly separate the effects of LLT and MNMT on the observed density fluctuations. Thus, we also investigated fluid Hg under high pressure and high temperature conditions, which shows MNMT near a critical point of LGT, to investigate how MNMT affects them. We observed distinct density fluctuations; a strength and a correlation length of them show maxima at around a critical isochore of LGT, and the former is basically consistent with a phase diagram (compressibility) of LGT; they do not show any peaks at MNMT region. Precise analysis revealed that MNMT only affects a shift of another parameter, a short-range correlation length. These results in fluid Hg indicate that the density fluctuations are mainly derived from a critical phenomena of LGT and MNMT does not play any critical role on them. We believe that the latter conclusion also holds true for liquid Te systems; MNMT plays no important role on the density fluctuations in liquid Te systems and LLT is the main origin of them.

Keywords: density fluctuations, small-angle x-ray scattering, liquid-liquid transition, liquid metal

(Some figures may appear in colour only in the online journal)

1. Introduction

To study density fluctuations in liquids, a small-angle x-ray scattering (SAXS) is a conventional and powerful tool. When it is applied to liquid metals, however, there is a critical problem. X-ray absorption coefficients of liquid metals are very high and thus both a strong (high-energy and high flux) x-ray source and a very thin sample are needed. Especially for supercritical fluids above a critical point of liquid–gas transition (LGT), which is a typical target of the study of

[4] Author to whom any correspondence should be addressed.

density fluctuations, high pressure and high temperature conditions are needed. Tamura and Inui have developed special techniques for x-ray measurements of high temperature and high pressure liquids using a synchrotron radiation to overcome this problem [1, 2]; they used resistive heaters [tungsten (W) or molybdenum (Mo) wires] and special sample cells made of sapphire (for Se and Hg) or single crystalline Mo (which was developed later by Matsuda [3]) (for alkali metals) to achieve high temperature state up to 1650 °C and He gas compression to high pressure state up to 200 MPa; they utilized SPring-8, a third-generation synchrotron radiation facility in Japan as a x-ray source; early days, they used Be windows in order to seal pressure and to transmit x-ray beams but later they updated them to diamond ones, which have much lower x-ray scattering intensity and thus enables them to obtain much better (lower signal to noise ratio) SAXS data. By using these techniques, their group succeeded to measure density fluctuations of many supercritical fluid metals: Hg [4] (critical point of LGT [5] is located at 1478 °C and 167.3 MPa), amalgams (Hg with small impurity of Bi [6] or Au), Se [7] (1615 °C and 38.5 MPa) and alkali metals [8, 9] (Rb (1744 °C and 12.45 MPa) and Cs (1651 °C and 9.25 MPa)).

In addition to LGT, it is very interesting to study density fluctuations corresponding to LLT. Liquid Te has been known to show some electric and thermodynamic anomalies and is proposed to have a continuous LLT. The possibility of LLT in liquid Te is first proposed [10] from electric anomalies. Solid Te is a typical semiconductor but an electric resistivity of liquid Te just above the melting point is poor metallic ($\simeq 1 \times 10^{-5}\,\Omega\,\mathrm{m}$) [11]. The temperature coefficient of the resistivity of liquid Te is negative [12, 13], which is opposite to that of normal metal. These anomalies were qualitatively explained by a two state model [10]; the resistivity consists of a semiconducting part and a metallic one and the fraction of metallic part increases with increasing temperature, which means that there is a continuous transition from semiconducting phase to metallic one. And later, the existence of LLT is discussed also from its thermodynamic anomalies [14]; the temperature dependence of density shows both maximum [15] and minimum [16] at just above the melting temperature ($T_\mathrm{m} = 450$ °C) and in a deep supercooled region (at around 290 °C), respectively. The temperature dependence of sound velocity shows minimum at around 360 °C, which is almost in the middle of the above mentioned two temperatures where density shows anomalies, and exhibits anomalous increase up to 800 °C [17]. At 360 °C, temperature dependence of specific heat capacity also shows maximum [18]. Pressure variation of melting curve shows maximum at around 1 GPa, which is also a supporting information to exist an LLT in liquid Te [19]. These features are much clearer in its mixtures. With adding Se, density [20] and velocity [21] curves shift to higher temperature, and all the three anomalies (density maximum, density minimum and velocity minimum) appear in the real liquid region (between the melting and the boiling temperatures) from about 30%–50% Se in mole fraction. Structural studies by x-ray or neutron and simulations told that these density anomalies are the result of continuous structural transition between 2-fold and 3-fold coordinated structures [22–24]. This continuous LLT also accompanies MNMT (or metal-semiconductor transition) [19, 25]. On the way of this LLT, corresponding density fluctuations should exist; Tsuchiya *et al* actually estimated the quantity of the density inhomogeneity from an anomalous temperature dependence of density and ultrasonic sound velocity in liquid Se–Te mixtures [26]. But a direct evidence of the density inhomogeneity has not been obtained for a long time until our recent SAXS measurement for liquid Se–Te mixtures [27]. Similar anomalies in density, ultrasonic and specific heat capacity were also observed in liquid Ge–Te mixtures [28] and therefore similar density fluctuations can be expected. On the other hand, a phase diagram of Ge–Te mixture has a eutectic point at 15% mole fraction of Ge and 375 °C (see also figure 6. Se–Te mixture is complete solid solution binary alloy). It is proposed that an eutectic point in a liquid binary alloy corresponds to something singular point in composition fluctuations [29, 30], which has never been directly verified by experiments. Also from this point of view, it is interesting to observe density fluctuations in liquid Ge–Te mixtures.

Liquid Si has been known as an anomalous liquid [31]. Solid (crystal) Si is a typical semiconductor but liquid Si shows metallic nature, which is similar to Te. It is believed that a remnant of solid structure should exist in liquid state and liquid Si has a inhomogeneous structure composed of a covalent-bonded solid-like structure and a non-bonded liquid-like one. Recent synchrotron based x-ray Compton scattering measurements provided results supporting it and liquid Si is proposed to be inhomogeneous in electronically [32, 33]. Thus also in liquid Si, LLT is proposed to exist in a deep supercooled region (transition temperature ∼800 °C [34], which is well below the melting temperature 1414 °C) and an *ab initio* simulation proposed that LLT of liquid Si accompanies MNMT [35]. It is also interesting to investigate whether this inhomogeneous structure can be detected by SAXS measurement.

What has been mentioned above are researches that have been conducted mainly in a field of liquid metals to understand the anomalous properties of liquid metals. On the other hand, when limited to thermodynamics, it has long been widely known that anomalies very similar to liquid Te are also found in liquid water [36], which is not of course liquid metal. The density shows maximum slightly above the melting temperature, the ultrasonic sound velocity anomalously increases with increasing temperature up to 80 °C. Anomalous increase of specific heat capacity is observed in a supercooled region [37, 38]. The melting temperature of water as a function of pressure has a negative slope, which is similar to that of Te above 1 GPa [19]. Furthermore, the solution that has been proposed to understand these anomalies of liquid water assumes LLT in deep supercooled region with its own critical point (liquid–liquid critical point (LLCP) hypothesis) [39, 40], which is also similar to liquid Te. The similarity between liquid Te and liquid water has come to be discussed by other researchers [41–43]. For liquid Si, an attention has also been paid to the similarity to liquid water which has a same

tetrahedrally-bonded structure in the crystalline state, and discussions have been made to understand both liquids with same LLCP hypothesis [34, 44]. The location of LLCP for liquid Si is also estimated [45]. From these similarities among liquid Te, Si and water, we believe that the anomalous properties seen in liquid Te and liquid Si are not material-dependent phenomena nor unique one to liquid metals, and are universal one associated with LLT including liquid water [27, 46, 47]. In the long term, we aim for a unified understanding of LLT and its effects on many properties of liquids. We believe that an inhomogeneity or a fluctuation is an essential property in LLT and thus we carried out SAXS measurements of some liquid metals to investigate such fluctuations in density. In liquid water, SAXS measurements have been carried out from early days [48–51] and it was revealed that SAXS intensity increases with decreasing temperature in the supercooled region. It should be an onset of LLT, however, there have been many arguments [52, 53] to interpret this experimental fact and the discussion of LLT scenario for liquid water had not been concluded (reviews: [54, 55]) for long time mainly because no one could reach to the other side of LLT by experiments. This problem was recently partially solved by SAXS measurement with using a latest technique of x-ray free electron laser [56], which enabled to obtain SAXS spectra within femtoseconds before the liquid water freezes. The experiment revealed that an integrated SAXS intensity shows maximum at around −44 °C, which should be a direct evidence of the existence of LLT or Widom line. Now the LLT model of liquid water becomes a hot topics again and a new type of discussion has started (see [57]).

The LLTs in the above mentioned liquid metal systems accompany MNMT, and we think that it is important to separate the effects of two transitions (structural and metal–nonmetal/semiconductor) on density fluctuations in order to construct a universal picture including liquid water. For this purpose, it is interesting to investigate supercritical Hg, which shows MNMT in the high temperature and high pressure conditions near an LGT critical point (1478 °C and 168 MPa [5]). By utilizing a supercritical state, a gradual expansion is achieved and the fluid metal becomes a non-metallic fluid on the way of this expansion. In fluid Hg, properties of electronic state (electric conductivity and Knight shift etc) are mainly dependent on density and MNMT is recognized to occur at around a density of 9 g cm^{-3} [5], which is slightly above a critical density of 5.8 g cm^{-3}. Inui *et al* already succeed to observe the density fluctuations [4] in supercritical fluid Hg, but the contributions from these LGT and MNMT were not well separated.

To apply SAXS techniques to such transition states of the liquid metals mentioned above, some improvements should be needed. The accuracy of the data must be much improved beyond Tamura and Inui's measurements because a strength of density fluctuations is expected to be much smaller in LLT sample than in supercritical fluid near an LGT critical point; the zero-wavenumber structure factor $S(0)$, which is a good parameter for the strength of density fluctuations, of the latter often reaches to 10^1 or larger but that of the former is less than 0.1. To explain more clearly, we indicate

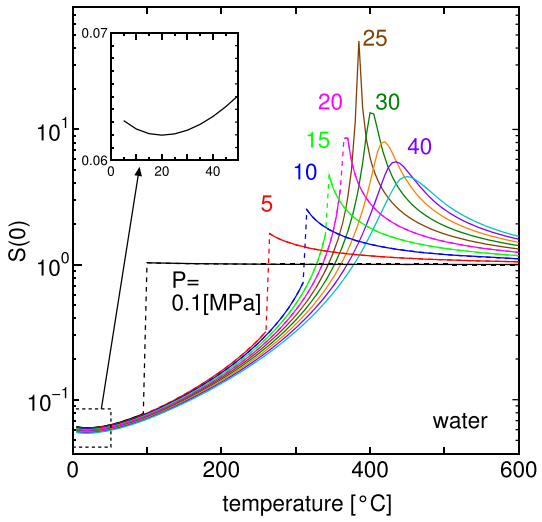

Figure 1. Temperature dependence of $S(0)$ of water at the pressures indicated in the figure.

$S(0)$ of liquid water estimated using thermodynamic quantities as an example. Water has an LGT critical point (374 °C and 22 MPa) and large density fluctuations are expected near the critical point. In figure 1, $S(0)$ of liquid water calculated by the following equation (ρ_N: number density, k_B: Boltzmann constant, β_T: isothermal compressibility) is plotted.

$$S(0) = \rho_N k_B T \beta_T \tag{1}$$

In this calculation, IAPWS (The International Association for the Properties of Water and Steam)-95 free energy formula [36] was used for the pressure dependence of density. Near the LGT critical point, an absolute value of $S(0)$ goes over 10^1. On the other hand, it is proposed that liquid water has an LLCP [39, 40] in a deep supercooled region. In the low temperature region (inset of figure 1), $S(0)$ shows increase with decreasing temperature, which is actually observed by the SAXS experiments [48–51]. It should be an onset of the LLT critical fluctuations. The discussion on a relation between the existence of LLCP and density fluctuations is not concluded [52–55], but an important fact here is that an absolute value of $S(0)$ for LLT is extremely small compared with that for LGT. This point has not been well considered in the discussion of LLT phenomena. Thus, it is very important to determine the absolute value of structure factor by SAXS experiments to discuss density fluctuations in LLT samples in detail.

For these purposes, we have improved the technique developed by Tamura and Inui [1], mainly a method of analysis: we treat the data very carefully and clarify some sources of the observed scattering intensity. Stability of a sample and a condition of incident beam are also improved. Although there still some technical problems, we can reveal tiny changes of SAXS intensities in some liquid metals, which has not been clarified before. After brief explanation about the experimental procedure in the next section, we present results of liquid Te systems including liquid Se–Te and Ge–Te mixtures, liquid Si and supercritical fluid Hg. Then we mention concluding

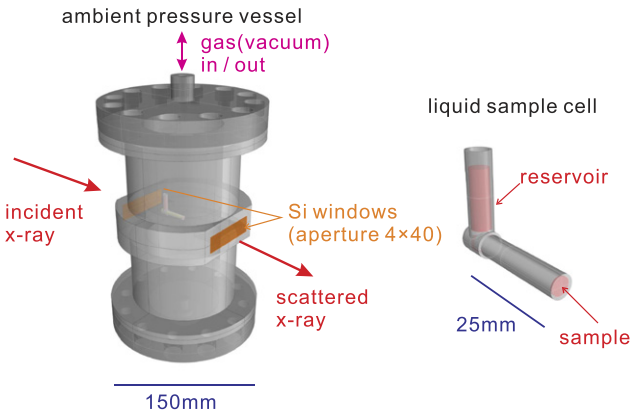

Figure 2. Schematic illustration of an ambient-pressure vessel and a liquid sample cell.

remarks. Details of the improvements in the experiments and data analysis are shown in the appendix.

2. Experiment

Liquid metal sample with a thickness of from about 200 to 600 μm, which were heated by Mo or W heaters, were installed in a poly- or single-crystalline sapphire cell. We used two types of vessels depending on the experimental conditions: one was a high pressure vessel with cylindrical-shaped single-crystalline diamond windows to allow a propagation of both incident and scattered x-rays, which has been used by Tamura and Inui [1, 2]; the other was an ambient pressure vessel with single-crystalline Si windows, which was newly developed. The outline of the latter vessel is illustrated in figure 2. The sample cell surrounded by the heat insulating ceramics (not shown in the figure) was held in the vessel. We used He gas as a pressure medium for these two vessels. SAXS measurements were performed using synchrotron radiation on a beamline BL04B2 at SPring-8, Japan. Schematic illustration of the beamline is presented in figure 3. The energy of the incident x-rays was set to 38 or 62 keV, by using Si (1 1 1) or Si (2 2 0) reflection as a monochrometer respectively. A small amount (5%–10%) of mixing of a higher harmonic x-ray, 114 or 124 keV for Si (1 1 1) or Si (2 2 0) respectively, was inevitable in this beamline because a single monochrometer without a mirror to eliminate high energy harmonics was used. Intensities of a incident and a transmitted x-rays were monitored by ionization chambers (IC) and the scattered x-rays were detected and accumulated for 20 min by imaging plate (IP, RIGAKU R-AXIS IV++) of size 300 × 300 mm^2 (3000 × 3000 pixel) located at a distance of 2.98 m from the sample position.

The IP was irradiated by x-rays scattered (directly) from a sample, a sapphire cell, and He gas, a fluorescence x-ray of sample element, and x-rays multiply scattered from a sample and He gas. We estimated these values and deduced a signal intensity from the sample. The intensity was normalized by a scattering intensity of He gas in the vessel without sample cell as a reference, and we thus obtained the absolute value of structure factor $S(Q)$ of the sample. Details of the data treatment is described in an appendix.

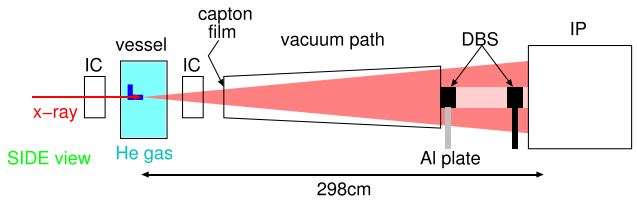

Figure 3. Schematic illustration of the SAXS experiment setup at beamline BL04B2, SPring-8.

3. Results and discussions

In this section, at first, we will show the results of liquid Te systems, which is a representative system of exhibiting LLT. The purpose to study this system is to obtain direct experimental evidence of density fluctuations induced by LLT. Results of Se–Te mixtures, Ge–Te mixtures and pure Te will be shown in separate subsections. Before going to other systems, we will shortly comment on density fluctuations of eutectic binary alloys because some discussion have been made on fluctuations of the system and Ge–Te mixture is also eutectic binary alloy. After that, we will show results of liquid Si, which is also expected to exhibit LLT. In the last subsection, we will indicate results of supercritical fluid Hg, which exhibits MNMT near its LGT critical point. The purpose is whether we can separate an effect of MNMT on the density fluctuations accompanying a critical phenomena of LGT.

3.1. Liquid Te systems

In liquid Te, LLT is supposed to exist at around 360 °C, which is 90 °C below a melting temperature. This temperature could be accessed with micro-samples in density measurement [16], however, it was difficult to reach in SAXS experiment, because it requires a large amount of sample and long measurement time. Therefore, we started experiments for its mixtures. When adding other elements (Se [20, 21, 25], Ge [28], etc), thermodynamic properties can be shifted to higher temperature and we can access the transition region above a melting temperature. We studied liquid Se–Te and Ge–Te mixtures not only due to an interest for fundamental features of these mixtures but also because it will be a prototype for supercooled liquid Te, water and Si, which cannot be accessed by normal experimental methods. We will show the results of these two mixtures above a melting temperature in the succeeding two subsubsections. Very recently, a new detector with much faster scan speed (1 min per 1 spectra) was introduced to the beamline. By using this detector, we carried out in-situ SAXS measurement of liquid Te during cooling below the melting temperature. We will shortly describe the preliminary results in the last subsubsection.

3.1.1. Liquid Se–Te mixtures. We have already reported the results of Se–Te mixtures in the previous paper [27]. The SAXS parameters (see equation (2)) change in conjunction with LLT, and $S(0)$ and the slope of $S(Q)$ as a function of temperature show peaks in the middle of the transition. When the sample is pressurized up to 100 MPa, the curves of density

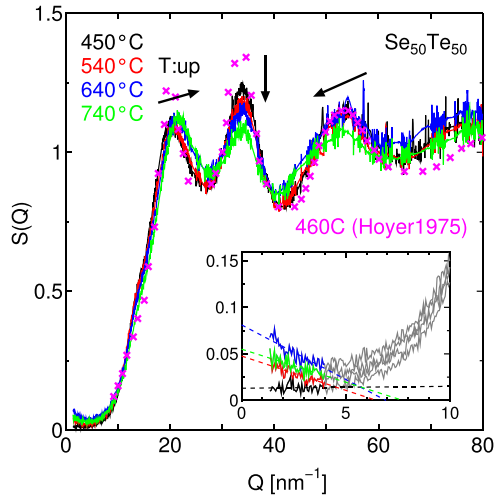

Figure 4. $S(Q)$ of liquid $Se_{50}Te_{50}$ at 450 (black line), 540 (red), 640 (blue) and 740 °C (green) by the present XD measurement. $S(Q)$ of XD at 460 °C by Hoyer is also plotted by pink crosses. Inset is an enlargement of a small Q region. Dashed lines are fitting results with linear function in a small Q region below 4 nm^{-1}.

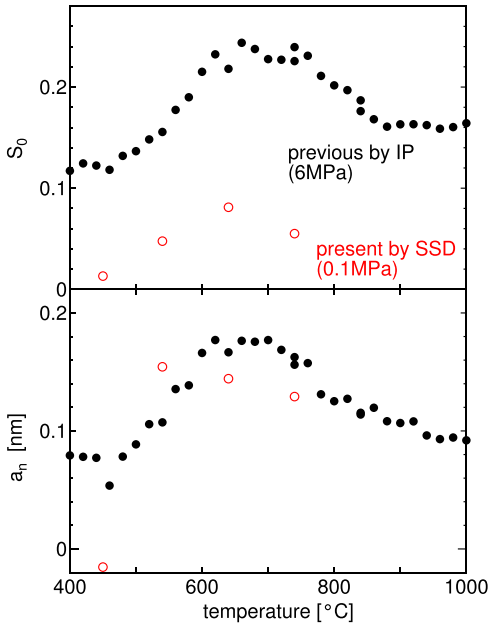

Figure 5. SAXS parameters (a) S_0 and (b) a_n of liquid $Se_{50}Te_{50}$. Red circles are estimated from a x-ray diffraction measurement with using SSD detector and black circles are from SAXS measurement with imaging plate.

and SAXS parameters shift to lower temperature. We concluded that we have succeeded in detecting density fluctuations derived from a continuous LLT. But in the previous measurement, we did not investigate whether the results were affected by the experimental conditions that the incident x-ray was not monochromatic but consisted of a basic (62 keV) and a small amount (5%–10%) of higher-harmonic (124 keV) components. Thus, it is better to check that this small amount of the higher-harmonic component does not give a critical effect to the conclusion. For this purpose, we carried out a x-ray diffraction (XD) measurement of liquid $Se_{50}Te_{50}$ at the same beamline (BL04B2 at SPring-8) by using a standard angle dispersive mode [58]. We used an SSD detector and a channel analyzer unit, which enabled us to extract the scattered x-ray with just only basic energy component (62 keV). In figure 4, we show structure factors of liquid $Se_{50}Te_{50}$ obtained by this XD measurement. Temperatures conditions of the sample are indicated in the figure. We can see three peaks at around 20, 34 and 54 nm^{-1} (hereafter we call these peaks a first, a second and a third peak, respectively). The present result at 450 °C, which is indicated by black line in the figure, is mostly consistent with a reported one at 460 °C by Hoyer [22], which is plotted by pink crosses. Positions of the peaks are almost consistent with each other. The intensities of the first and the second peaks in the present result, however, are slightly smaller than those by Hoyer. When the temperature is raised from 460 °C to 740 °C, the first peak position shifts to higher Q and the intensity increases slightly; the second peak position hardly changes but the intensity largely decreases; the third peak position shifts to lower Q and the intensity decreases slightly. These changes are almost consistent with a temperature variation of $S(Q)$ estimated from an inelastic neutron scattering experiment by Chiba [59]. As shown in the inset of figure 4, $S(Q)$ in a small Q region below 4 nm^{-1} is almost flat at 450 °C as indicated by a black line. When the temperature is raised up to 640 °C, which is indicated by a blue line, $S(Q)$ at a small angle gradually increases. But when the temperature is further raised to 740 °C, it decreases as indicated by a red line. To clarify the temperature variation of these SAXS results, we fit $S(Q)$ below 4 nm^{-1} by a linear function as,

$$S(Q) = S_0(1 - a_n Q). \tag{2}$$

S_0 is a structure factor in the zero wavenumber limit and a_n is a slope of $S(Q)$ normalized by S_0, which is related with a spatial size of density fluctuations. We plot these SAXS parameters in figure 5 by red open circles. Both of S_0 and a_n show maxima at 640 °C, which is almost in the middle of LLT region. Thus we can confirm that the main conclusion of the previous paper [27]: the strength and the spatial size of density fluctuations of liquid $Se_{50}Te_{50}$ as a function of temperature show maximum in conjunction with LLT. However, a quantity of S_0 is well smaller than that by the previous measurement, which is indicated by black circles in the same figure. We are not sure the origin of this discrepancy at the present stage. It is useful to compare S_0 parameter with $S(0)$ calculated by a compressibility using (1), but it is difficult because there is no reliable data on a pressure dependence of density for this mixture and strictly speaking, (1) is not correct for mixtures. The discrepancy may come from a difficulty to determine the absolute value of $S(Q)$ in such a small Q region by a standard XD experiment or may due to an incompleteness of the present SAXS measurement system by IP. We will continue further investigation in the future.

3.1.2. Liquid Ge–Te mixtures. Next, we report results of liquid Ge–Te mixtures. In figure 6, we show a phase diagram of Ge–Te system in a low x (mole fraction of Ge). In this system, there is a eutectic point at around $x = 0.15$ and $T = 375$ °C. In pure Te, a density shows maximum and minimum just above

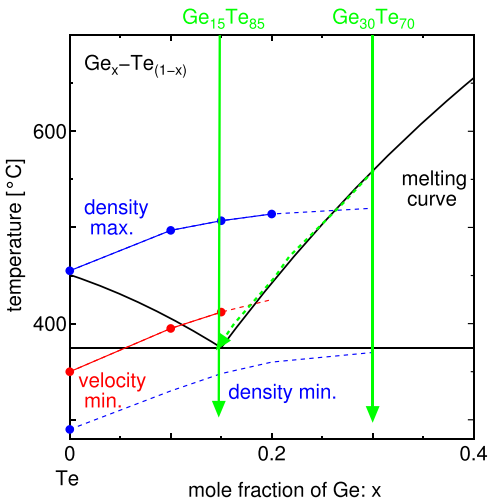

Figure 6. Phase diagram of Ge–Te system in a small x region. There is a eutectic point at around $x = 0.15$ and $T = 375$ °C. The loci of density minimum/maximum and sound velocity minimum [28] are shown by blue lines and red one, respectively.

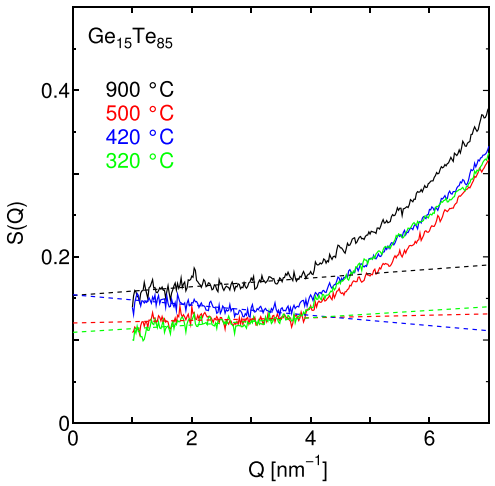

Figure 7. $S(Q)$ of liquid $Ge_{15}Te_{85}$ at an ambient pressure. Temperatures are 900 (black), 500 (red), 420 (blue) and 320 (green) °C. Dashed lines are fits by an equation (2) in a small Q region below 3.5 nm^{-1}.

the melting temperature and in a deep supercooled region [16] respectively, and a sound velocity shows minimum [21] in a supercooled region. These loci are important signatures in drawing a phase diagram of LLT: the loci of density maximum and minimum can be recognized as a high- and a low-temperature ends of the transition respectively, because a negative thermal expansion, which is thermodynamically anomalous, appears between them; the locus of velocity minimum can be recognized as a center of the transition because it actually locates almost in the center of the above mentioned loci of density anomalies. By adding Ge, the loci of density maximum and velocity minimum shift to higher temperatures [28], as plotted in figure 6. (We limit the discussion to Te-rich mixture here, because the situation seems to become different when a fraction of Ge increases over $x \geqslant 0.4$ [28].)

We have carried out (simultaneous) density and SAXS measurements for $x = 0.15$ and $x = 0.30$ samples by using an ambient pressure vessel. Figure 7 shows a temperature variation of $S(Q)$ of liquid $Ge_{15}Te_{85}$ mixture in a cooling process. At the highest temperature (900 °C), an absolute value of $S(Q)$ is relatively high but a slope in a small Q region (<3.5 nm^{-1}) is moderate. When decreasing the temperature down to 500 °C, the absolute value of $S(Q)$ decreases on the whole Q but the shape is basically not changed. Further decreasing the temperature to 420 °C, however, the shape is changed especially at $Q < 4$nm^{-1}. The slope becomes relatively steeper and the $S(Q \to 0)$ value becomes larger. When the temperature is further decreased down to 320 °C, which is a supercooled state ($T_m = 375$ °C), the slope becomes moderate again. Below this temperature, the sample was frozen to a solid. This temperature variation of $S(Q)$ clearly proves that a strength of density fluctuations becomes maximum at around 420 °C according to a continuous LLT. To clarify the temperature change of density fluctuations, we fitted $S(Q)$ in a small Q region below 3.5 nm^{-1} by an equation (2). Figure 8 shows temperature dependences of (a) density, (b) S_0 and (c) a_n for (1) $Ge_{15}Te_{85}$ and (2) $Ge_{30}Te_{70}$. In the measurements, at first we melted and entered the sample into a thin space of sapphire cell at slightly above a melting temperature (400 °C for $Ge_{15}Te_{85}$ and 650 °C for $Ge_{30}Te_{70}$). After that, we increase the temperature up to 900 °C and decrease it, finally down below 350 °C to solidify the sample. The reproducibility of the parameters are satisfactory well for both of a heating-up and a cooling-down process. In $Ge_{15}Te_{85}$, the density indicates positive slope (negative expansion) as a function of temperature from 350 °C to 500 °C, where the sample shows continuous phase transition between a low- and a high- density phases. At higher temperatures above 600 °C, S_0 shows slight increase, which should be a tail of critical density fluctuations of LGT. On the other hand, almost in the middle of the above mentioned two temperatures (420 °C), SAXS parameters (S_0 an a_n) show maxima, which clearly indicates that there are density fluctuations due to LLT. The sample solidifies at about 300 °C, which is well below the melting temperature, and the density jumps to a higher value (5.40–6.05 g cm^{-3}). SAXS parameters also jump to higher values, which indicates that the sample changes to a poly-crystalline state or glass, not to a crystal with large grain sizes.

In $Ge_{30}Te_{70}$, there is a solid-liquid coexisting two phase region between 375 and 560 °C in a phase diagram (see figure 6). In figure 8, the density (2a) shows normal negative slope and S_0 (2b) show moderate positive slope in an one-phase liquid region above 530 °C (slightly supercooled) as a function of temperature. Below 530 °C, the sample stays in the solid–liquid two-phase state. In figure 9, we show SAXS images of $Ge_{30}Te_{70}$.

In the measurements of Ge–Te mixtures, the normal pressure vessel equipped with rectangular windows was used. This means that we can see a rectangular bright area in all the images in figure 9(a) At 560 °C, the image shows halo patterns, which is typical for liquid. When decreasing temperature to 520 °C, spotty patterns appears, which indicates that there is a small, but macroscopic, crystalline piece in the sample and the sample becomes solid–liquid two-phase state. At 520 °C, the density also shows small jump, which should be

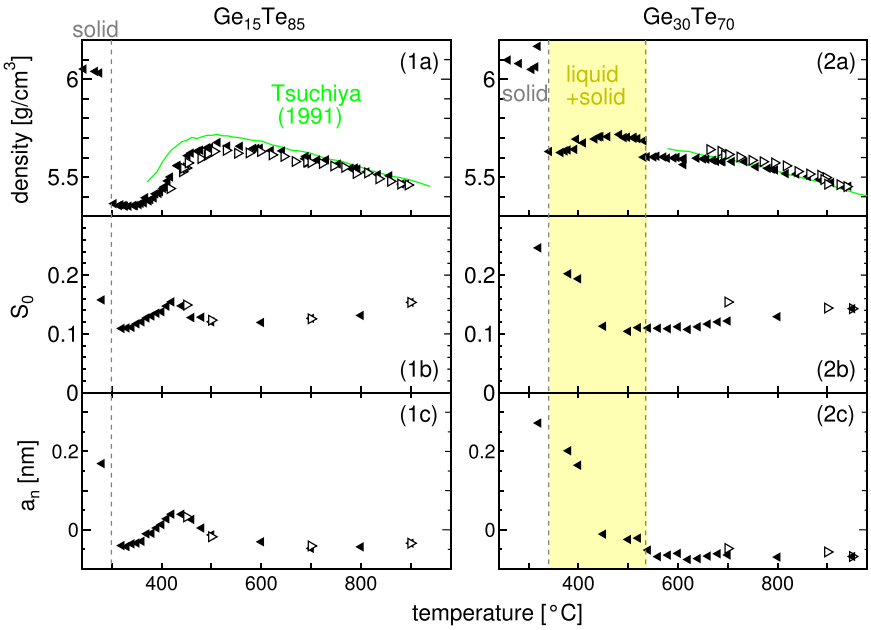

Figure 8. (a) Density and SAXS parameters ((b) S_0 and (c) a_n) for liquid (1) $Ge_{15}Te_{85}$ and (2) $Ge_{30}Te_{70}$. Right (increase temperature) and left (decrease) headed triangles indicate the direction of temperature change of the measurement. Green solid lines are reference value at ambient pressure [28].

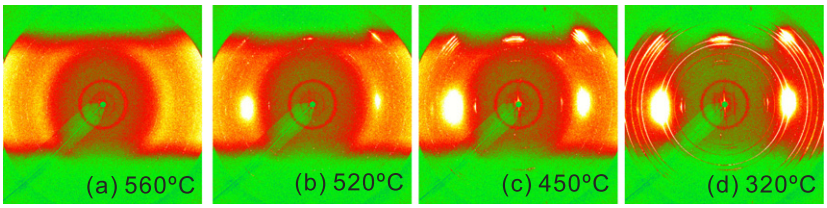

Figure 9. SAXS spectra of $Ge_{30}Te_{70}$ at (a) 560, (b) 520, (c) 450 and (d) 320 °C. A scattering intensity from the sample is limited in a square region due to a slit window of the vessel.

smooth and we do not have a reasonable explanation. Further decrease the temperature in this two-phase region, these spotty patterns grow at (c) 450 °C, which means that a size of the macroscopic crystalline piece grows. In this temperature, not only the spotty patters but also spiky ones appear in the center of the image, which we remove in $S(Q)$ analysis. The SAXS parameters in figures 8(2b) and (2c) show much increase with decreasing temperature, which indicates that density fluctuations in the coexisting liquid phase becomes distinct. In the two-phase region, the coexisting liquid phase basically changes the state along a melting line such as indicated by a green dashed line in figure 6. Hence, it is reasonable that this coexisting liquid phase shows density fluctuations below about 500 °C. Finally at 320 °C (figure 9(d)), the sample becomes frozen to a poly-crystalline solid and it appears a ring pattern of Bragg diffraction.

3.1.3. Liquid Te. In the above two subsubsections, we described SAXS results of Se–Te and Ge–Te mixtures. From these results, it is almost certain that pure liquid Te also has density fluctuations associated with LLT. Results of inelastic x-ray scattering experiment of liquid Te also suggest to exist a structural inhomogeneity [46, 60] in the sample. However, in fact, we could not detect any significant changes in the previous SAXS measurement of pure liquid Te [27]. We concluded that density fluctuations in pure Te were smaller than our experimental accuracy because we just measured above the melting temperature and did not reach to the real transition region located in its deep supercooled region. To solve this problem, we recently carried out SAXS measurement of pure liquid Te again by using a new detector (PerkinElmer, XRD1621AN3); it enabled us to obtain SAXS spectra with enough accuracy in about 1 min, which is greatly improved compared that with imaging plate which needs about 20 min to take one spectra. When the measurement time becomes so short, it becomes possible to perform an *in situ* measurement during cooling below the melting temperature. By using this detector, we actually succeeded to obtain SAXS spectra down to a low temperature of 150 °C below the melting temperature. The obtained SAXS intensity showed maximum at around 350 °C which is almost in the middle of the LLT region in liquid Te. We will report this result in near future.

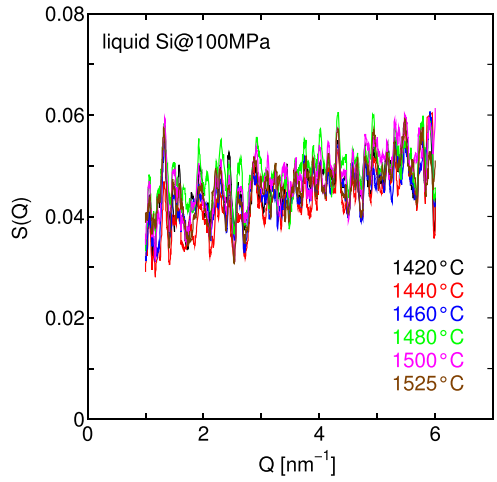

Figure 10. $S(Q)$ of liquid Si. Temperatures are indicated in the figure.

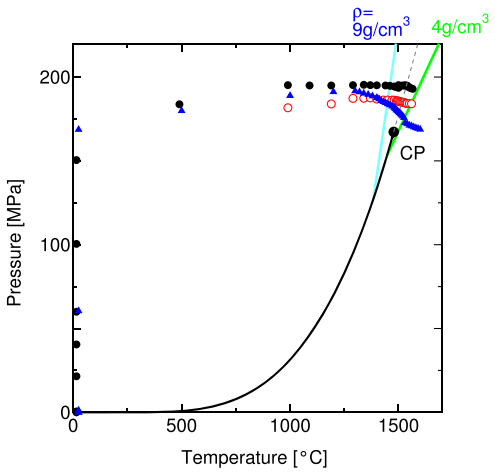

Figure 11. State points of the SAXS measurements for fluid Hg. Black and red symbols are the results by incident x-ray energy of 62 keV and blue ones are by that of 38 keV. CP denotes LGT critical point. Bold- and thin-dashed-lines indicate a coexistence curve and a critical isochore (5.8 g cm^{-3}), respectively. Blue and green lines are isochores of 9 and 4 g cm^{-3}.

3.2. Comments on liquid eutectic binary alloy

It is proposed that an eutectic point in liquid binary alloy corresponds to a something singular point in composition fluctuations [29, 30]. This scenario is, however, not true at least for Ge–Te binary alloy. As shown in section 3.1.2, distinct changes were observed in the parameters of density fluctuations for the eutectic composition ($Ge_{15}Te_{85}$) but the strength and the spatial size of density fluctuations show maxima at 420 °C, which is well above the eutectic temperature (375 °C); we concluded that the density fluctuations in $Ge_{15}Te_{85}$ arise from LLT in liquid Te not from the singularity of eutectic point of $Ge_{15}Te_{85}$. We also carried out SAXS measurements for liquid Pb–Sn alloy system which also has a eutectic point at 74% mole fraction of Sn and 183 °C and reported tentative results [61]. The temperature change of density fluctuations we observed for the eutectic composition sample was very small, which did not show a divergence at the eutectic point. The temperature dependences of density fluctuations are rather evident for non-eutectic composition samples. We now continue further investigation for Pb–Sn system to prove that the eutectic point is not a singular point.

3.3. Liquid Si

To detect density fluctuations derived from LLT, we have carried out a SAXS measurement of liquid Si. In this measurement, an energy of incident x-ray was 38 keV. Figure 10 shows a temperature variation of $S(Q)$ of liquid Si. In conclusion, we could not detect any effective temperature change of the spectra. We believe that there is density inhomogeneity or LLT in liquid Si, but density fluctuations are so tiny as not to detect them in the present experimental accuracy and in the present temperature region far above LLT.

3.4. Supercritical fluid Hg

In supercritical fluid Hg, the location of MNMT (density is about 9 g cm^{-3}) is well different from that of LGT (critical density is 5.8 g cm^{-3}) and thus, it is supposed to be possible, in principle, to separate effects of these two transitions on density fluctuations. This fact is different from supercritical fluid alkali metals, which was revealed by the experiment [5], and fluid hydrogen by simulation [62], whose locations of MNMT are almost coincide with those of LGT. Inui *et al* already succeeded to detect density fluctuations of supercritical fluid Hg [4], but contributions from these MNMT and LGT were not well separated. After that, the experimental techniques have been much improved, and thus we have carried out SAXS measurements of supercritical fluid Hg again by using a x-ray with energies of 62 keV and 38 keV as incident beams (only 38 keV in the previous experiment [4]). Figure 11 indicates the pressure and temperature conditions of the measurements in a phase diagram of fluid Hg. Isochores of density 9 and 4 g cm^{-3} where electric conductivities σ are 2×10^2 and 1×10^{-3}S, respectively, are plotted by a blue and a green lines in the figure. State points of the measurements cover from a full-metallic ($\sigma > 2 \times 10^2$) state to a full-nonmetallic ($\sigma < 1 \times 10^{-3}$) one. The measurements are carried out with increasing temperature at almost constant pressures above a critical pressure with an incident x-ray energy of 62 keV (indicated by black and red symbols in the figure) and 38 keV (blue symbols). Figure 12 shows the representative results of $S(Q)$ at pressure about 185 MPa and temperatures indicated in the figure. At 1000 °C, $S(Q)$ is almost flat and shows smaller value. With increasing temperature, $S(Q)$ in a small Q region grows and a slope of the curve becomes steeper due to critical density fluctuations of LGT. Beyond 1515 °C, where the density is critical (5.8 g cm^{-3}), the intensity and the slope of $S(Q)$ becomes decreasing. We fit $S(Q)$ by an Ornstein–Zernike function, $S(Q) = S_0/(1 + \xi^2 Q^2)$. To clarify the temperature dependence of the sample state, we plotted all these parameters in figure 13. The estimated (a) densities (symbols) are consistent with those calculated according to a literature (solid lines) [5]. The estimated (b) S_0 values

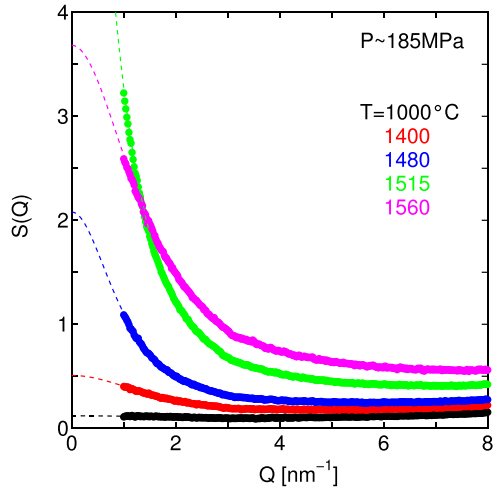

Figure 12. $S(Q)$ of fluid Hg at pressure 185 MPa and temperatures indicated in the figure.

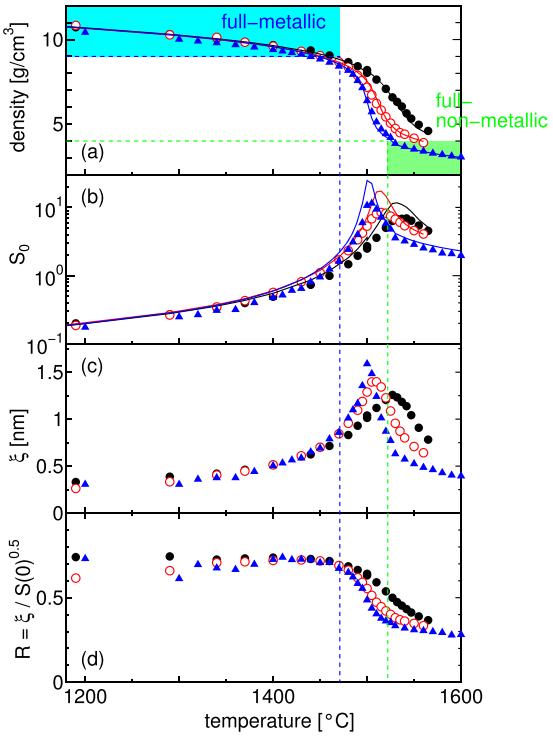

Figure 13. Temperature dependences of (a) density, (b) S_0, (c) ξ and (d) short correlation length R of fluid Hg. Black, red and blue symbols correspond to those in figure 11. Black, blue and red lines are calculated values according to a literature [5].

show peaks at around a isochore line of critical density, which indicate the observed density fluctuations are derived from LGT. In the present accuracy, we cannot comment on a small discrepancy between a critical isochore line and a ridge line (maximum line of fluctuations), which has been discussed for supercritical liquid water [63] and supercritical fluid hydrogen [62]. The quantities of experimentally estimated S_0 are basically consistent with those calculated by an equation (1) using parameters in a literature [5], but the formers are slightly smaller than the latter in a high-S_0 region. We know that there is a slight temperature gradient in our sample cell, which may suppress the critical fluctuations. Or a small amount of a high-energy x-ray in the incident beam may affect this discrepancy. An Ornstein–Zernike correlation length ξ indicated in figure 13(c) shows similar temperature dependence as S_0. The interesting parameter is a short-range correlation length (figure 13(d)), which is defined by $R = \xi/\sqrt{S_0}$ [64]. This parameter abolishes a diverging nature of ξ due to critical density fluctuations and can extract a higher order information concerning about a correlation beyond a local structure. In a low temperature region below 1475 °C, where the sample is full-metallic state, R is nearly constant 0.75. Above this temperature, R gradually decrease and finally seems to converge to a constant value 0.3 in a high temperature region, where the sample becomes full-nonmetallic state. In the previous study [4], the accuracy of the data was not good in the low temperature region (where there exist small density fluctuations) and the discussion was not clear. The present study give a clear result that MNMT induces a shift of R from a higher value which correspond to fluid metal, to a lower one to nonmetallic fluid. It does not show a peak at MNMT.

Finally, we comment on a mechanism of MNMT in fluid metals. In fluid Hg, a band-overlap model (so-called Bloch–Wilson model) was proposed to explain the continuous MNMT (see details in the review papers: section 2.3 in [5] and section 3.3 in [1]). But early results obtained by this simple picture led us to a deep forest; it could not explain all the properties relating with MNMT in fluid Hg such as a location (density) of MNMT, Knight-shift value, optical and electrical conductivity gaps and optical absorption. We suspect that there may be a critical flaw to apply the band model, which has been successful with crystalline materials, into fluids or liquids; basically it does not take into account a heterogeneity in a sample. The present SAXS results for fluid Hg clearly proves that at MNMT region, there exists distinct heterogeneity in density, that also naturally means heterogeneity in metallic nature. We believe that this heterogeneity is essential to discuss MNMT in liquid systems because the existence is also directly proved by the experiment in liquid chalcogenides (present results) and fluid alkali metals [8] at MNMT region. We expect other type of study which enables to consider this heterogeneity; advanced version of percolation model [65] or much larger size version of *ab initio* simulation ([66, 67]), which enable to consider mesoscopic heterogeneity, may be the candidates.

4. Concluding remarks

We have improved SAXS techniques succeeding to those installed by Tamura and Inui, applied it for some liquid metals to investigate a relation between density fluctuations and transitions such as LLT, LGT and MNMT. In liquid Se–Te and Ge–Te mixtures, which show continuous LLT accompanying MNMT, a strength and a spatial size of density fluctuations changed in conjunction with LLT and their

temperature dependences showed peaks in the middle of the transition. It is first direct evidences of density fluctuations associated with LLT. In liquid Si, we could not detect any changes corresponding to LLT in the present experimental accuracy. We concluded that it is because the real transition in this system locates in a deep supercooled region and the effect of it is very small at around the melting temperature. In supercritical fluid Hg, which shows MNMT near a critical point of LGT, distinct density fluctuations were observed and a strength and an Ornstein–Zernike correlation length show peaks at around a critical isochore of LGT. The strength of density fluctuations was basically explained by an isothermal compressibility calculated from a phase diagram of fluid Hg, which means that the density fluctuations are mainly due to critical density fluctuations of LGT. MNMT near LGT in fluid Hg just affects on an another parameter of density fluctuations; it gives a shift of a short-range correlation length R. From these results, we concluded that in liquid or fluid metals, MNMT has a negligible effect and LLT and LGT play leading roles on density fluctuations; in this sense, metallic and non-metallic liquids cannot be distinguished with respect to LLT. This conclusion is very important to discuss the similarity between the thermodynamic anomalies of liquid Te and those of liquid water and to construct the unifying framework of LLT phenomena [42, 46, 47] in the future.

Acknowledgment

This work was supported by JSPS KAKENHI Grant Numbers 20740223, 24740265 and 20244061. The synchrotron radiation experiments were performed at SPring-8 with the approval of the Japan Synchrotron Radiation Research Institute (JASRI) (Proposal Nos. 2007A1670, 2008A1138, 2011B1342, 2011B1486, 2012A1352)

Appendix A. Details of data treatment

In this section, we show the details of data treatment how to analyze structure factor $S(Q)$ of liquid samples from the observed SAXS spectra. Figure A1 shows representative IP images of SAXS experiments for (a) an empty cell at 6 MPa (compressed He gas) and room temperature and (b) liquid Te at 6 MPa and 500 °C by using a high-pressure vessel and an incident x-ray of 62 keV in energy. In figure A1(a), almost flat scattering intensity (see also figure A2) is observed except a diffraction ring near a center position. This diffraction pattern comes from kapton film used for a vacuum path. In figure A1(b), a bright pattern which comes from a liquid sample is limited in an off-centered circle area because an aperture of a scattering window of a high-pressure vessel is small (effective radius of 4 mm). The shaded area in the left-bottom direction from the center is due to a thin (thickness of 2 mm) Al plate just behind a vacuum path, which we used to estimate a fluorescence intensity from the sample. We analyzed the data separately by inside/outside and with/without Al plate regions as indicated in figure A1(c). Figure A2 indicate the corresponding SAXS profile (momentum-transfer dependence of the observed intensity) of (a) an empty cell and (b) liquid Te. In these figures, profiles $I^{(i)}_{\rm smpl}$ (i = 1, 2, 3) correspond to regions (1), (2) and (3). In an empty cell (figure 15(a)), the peaks of $I^{(1)}_{\rm cell}$ at 1.8, 3.6 and 7.2 nm^{-1} indicate diffraction patterns from the kapton sheet of the vacuum path; 3.6 and 7.2 nm^{-1} correspond to an incident x-ray of 62 keV and 1.8 nm^{-1} correspond to a higher harmonic x-ray of 124 keV. We estimated a ratio of the higher harmonic x-ray is about 7% ($x_{\rm 124keV} = 0.07$) in the total x-ray intensity from the area of these two peaks at 1.8 and 3.6 nm^{-1}. A spiky peak at 9 nm^{-1} is a diffraction peak from a poly-crystalline sapphire cell. The profile $I^{(2)}_{\rm cell}$ (with Al plate) is slightly lower than $I^{(1)}_{\rm cell}$ (without Al plate), which is well explained by a transmission of Al plate for an incident x-ray ($T_{\rm Al}(E_{\rm in} = 62\,{\rm keV}) = 0.9$). But in liquid Te (figure A2(b)), $I^{(2)}_{\rm smpl}$ is much lower than $I^{(1)}_{\rm smpl} \times 0.9$. We conclude that the observed intensity includes fluorescence x-rays from Te because the energy of incident x-ray is not so high from K-edge of Te (31 keV). We estimated the fluorescence intensity of sample $Y_{\rm fl}$ as,

$$Y_{\rm fl} = \left(I^{(1)}_{\rm smpl} - \frac{I^{(2)}_{\rm smpl}}{T_{\rm Al}(E_{\rm in})} \right) \frac{T_{\rm Al}(E_{\rm in})}{T_{\rm Al}(E_{\rm in}) - T_{\rm Al}(E_{\rm fl})} \qquad \text{(A.1)}$$

where $T_{\rm Al}(E_{\rm fl})$ is the transmission of an Al plate at the fluorescence energy ($E_{\rm fl}$ = 27 keV for K_α fluorescence of Te). In the measurement of fluid Hg, this value is almost zero because K-edge of Hg (83 keV) is well higher than the energy of incident x-ray, which is consistent that the origin of the value is fluorescence x-rays from Te.

Figure A3(a) shows the background subtraction (with considering the transmission of the sample $T_{\rm smpl}$) spectra of liquid Te corresponding to figure A1. The intensity outside the aperture of the scattering window should be zero because a scattering from sample is limited inside the window, but it is not actually. Figure A3(b) shows the corresponding profile of region (3) (outside window without an Al plate). Background (emptycell and He gas) subtracted profile (red line) indicates finite value, and almost Q-independent profile. A conceivable origin of the profile is the x-ray intensity multiply scattered by He gas after scattered by a liquid sample. We fit this profile by a linear function and decided this multiply scattered intensity as $Y_{\rm multi} = (I^{(3)}_{\rm smpl} - I^{(3)}_{\rm cell} T_{\rm smpl})$.

Thus, we deduced the scattering intensity of the sample, $Y_{\rm scat}$, as the following equation.

$$Y_{\rm scat} = I^{(1)}_{\rm smpl} - I^{(1)}_{\rm cell} T_{\rm smpl} - Y_{\rm fl} - Y_{\rm multi}. \qquad \text{(A.2)}$$

Note that we used three different values of $T_{\rm smpl}$; 0.315 for the kapton diffraction peak at 3.6 and 7.2 nm^{-1} which is the transmission of sample at 62 keV; 0.832 for the kapton diffraction peak at 1.8 nm^{-1} which is that at 124 keV; $0.35 = 0.832 \times x_{\rm 124keV} + 0.315 \times (1.00 - x_{\rm 124keV})$ for other area. Deduced scattering intensity from the sample and other estimated profiles are shown in figure A4. At 5 nm^{-1}, a

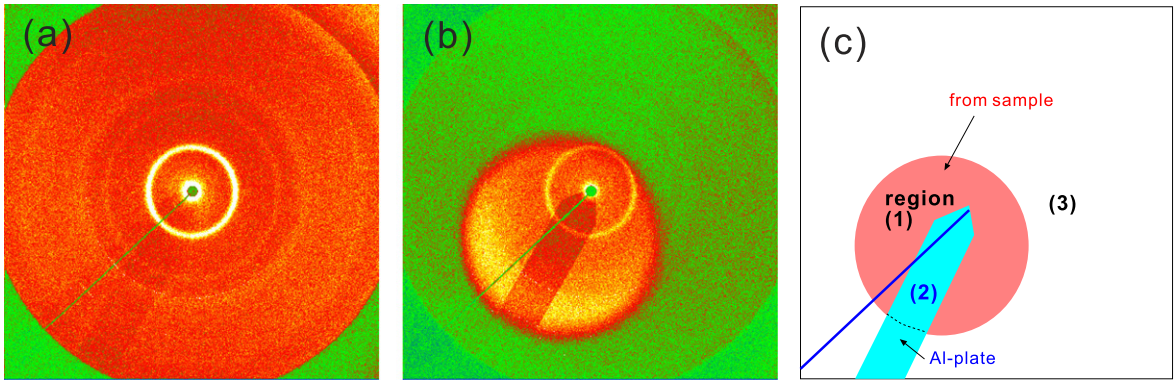

Figure A1. SAXS images of (a) a empty cell at 6 MPa and (b) liquid Te at 6 MPa and 500 °C. (c) indicates a schematic illustration of analyzed regions.

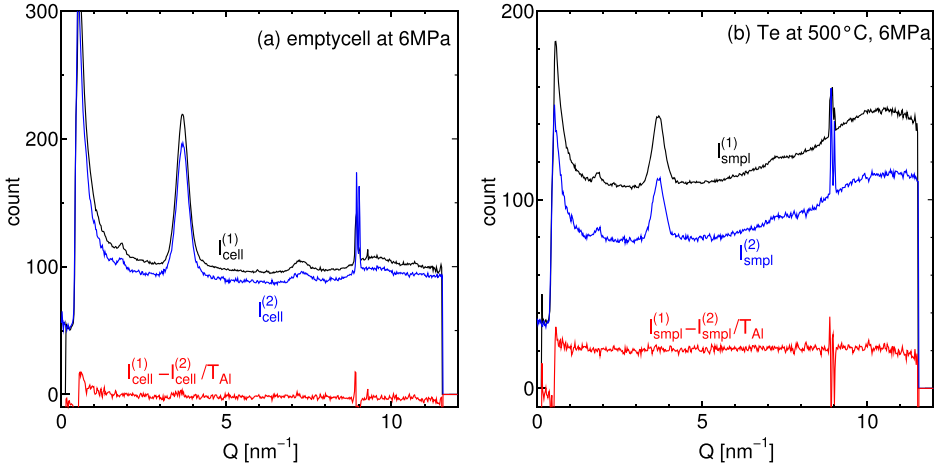

Figure A2. SAXS profiles of (a) empty cell and (b) liquid Te corresponding to those in figure A1.

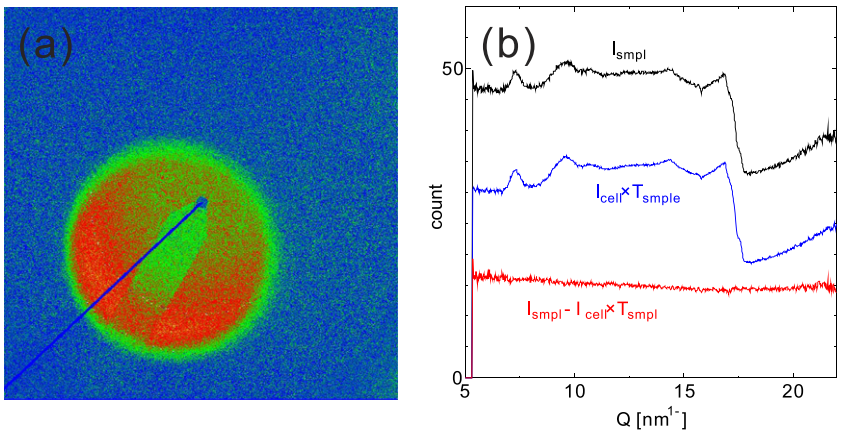

Figure A3. Background subtracted (a) image and (b) profile. The sample and background data correspond to those in figure A1.

real count scattered from the sample (Y_{scat}) is only about 15 in the total measured count is about 110 (I_{smpl}). What we have extracted by this procedure is thus the scattering intensity from the sample with the x-ray composed of 93% 62 keV and 7% 124 keV.

To obtain the absolute value of scattering factor $S(Q)$ from this scattering intensity, we have to decide the normalizing constant C.

$$Y_{smpl}(Q) \approx CNT_{smpl}T_{He}S(Q) \quad \text{(for small } Q\text{)} \qquad \text{(A.3)}$$

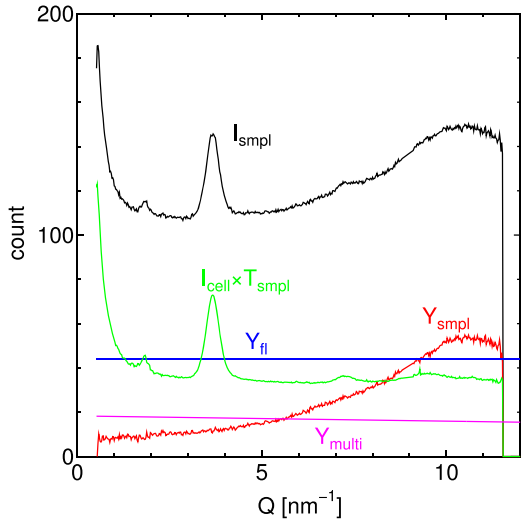

Figure A4. A scattering intensity from sample and other elements.

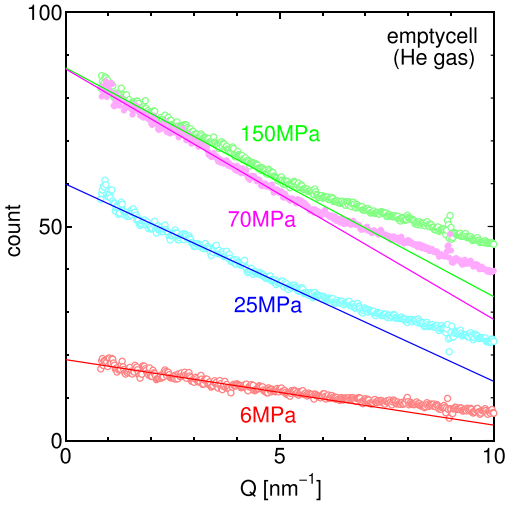

Figure A5. Pressure variation of scattering profile of He gas.

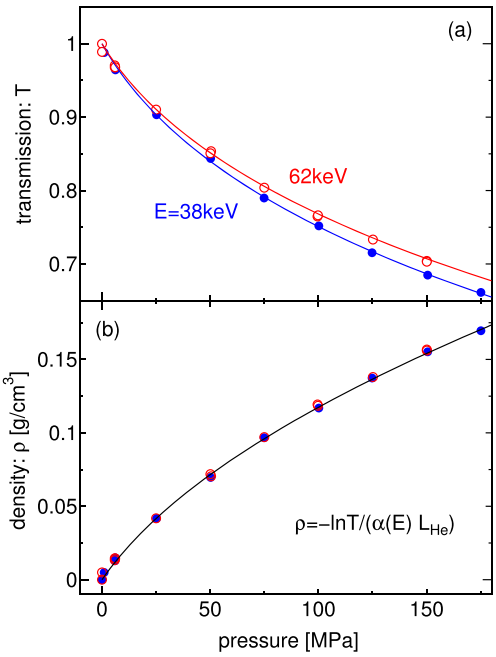

Figure A6. Pressure dependences of (a) transmissions and (b) densities of He gas. Blue and red symbols represent the data at incident x-ray energy 38 and 62 keV, respectively. Solid lines are calculated values by an equation (A.4).

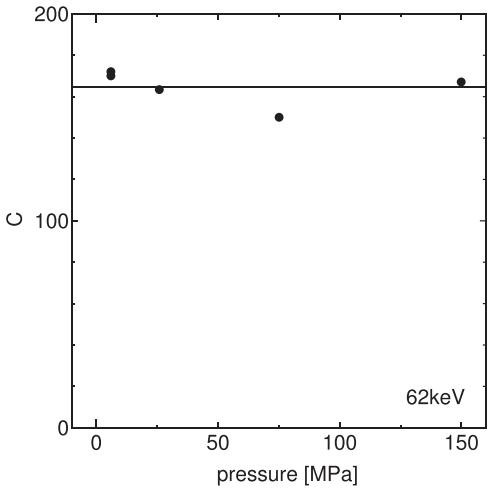

Figure A7. Normalizing constant C estimated from a compressibility of He gas.

where N is number of the sample particles. We used compressed He gas as a reference and determined C by the thermodynamic equation of He gas, $Y_{\mathrm{He}}(Q=0) = CN_{\mathrm{He}}S_{\mathrm{He}}(Q=0) = CN_{\mathrm{He}}\rho_N k_{\mathrm{B}}T\beta_T^{\mathrm{He}}$. Figure A5 shows scattering intensities of He gas at pressures in the figure which is deduced by subtracting emptycell data at vacuum condition as $Y_{\mathrm{He}} = I_{\mathrm{cell}}^{(1)}(P) - I_{\mathrm{cell}}^{(1)}(P=0)\times T_{\mathrm{He}}$. We fit Y_{He} in the small Q-region ($Q < 5$) nm^{-1} by a linear function and estimated $Y_{\mathrm{He}}(Q=0)$ (figure A6). On the other hand, we calculate $S_{\mathrm{He}}(Q)$ by a compressibility of He gas. shows pressure variations of (a) the transmission and (b) the density of He gas at 25 °C decided by this experiment. Blue and red symbols correspond to the data by incident x-ray energies 38 and 62 keV, respectively. The densities estimated by these two incident energies well coincide with each other. We assume a virial equation for the pressure [P (MPa)] dependence of He density [ρ_{He} (g cm^{-3})] and determined the virial coefficients as,

$$P = \frac{RT}{M}\left(a_1\rho_{\mathrm{He}} + a_2\rho_{\mathrm{He}}^2\right), \quad a_1 = 0.745371,\ a_2 = 5.36043. \tag{A.4.}$$

where $R = 8.3145$ (J K$-^1$ mol) and $M = 4.0026$ are gas constant and atomic mass of He, respectively. Calculated values of density and transmission of He gas with using this virial equation were plotted in 19 by solid lines, which well reproduce the experimental values. Figure A7 indicates a normalizing constant C estimated by the above procedure. C is almost independent on pressure and we adopted the averaged value of 165 as a normalizing constant. Figure A8 shows the structure factors $S(Q)$s of liquid Te at temperatures 500, 700 and

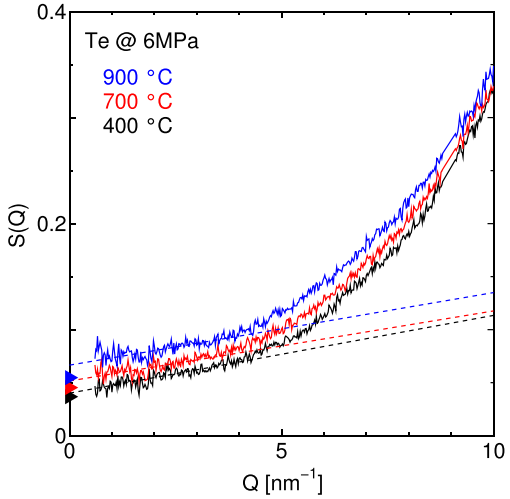

Figure A8. Temperature variation of $S(Q)$ in liquid Te. Triangle symbols at $Q = 0$ are $S(0)$ values calculated from a compressibility of liquid Te [68]. Dashed-lines are fitting results using of linear function in a small Q region ($Q < 4$ nm^{-1}).

900 °C by using this normalizing constant C. The absolute values of these $S(Q)$s are almost consistent with those calculated from a compressibility [68] as $S(0) = \rho_{\mathrm{N}}^{Te} k_{\mathrm{B}} T \beta_T^{\mathrm{Te}}$ indicated by triangles in the figure.

We concluded that we can determine the absolute value of small-angle structure factor.

ORCID iDs

Y Kajihara https://orcid.org/0000-0003-4920-6029
M Inui https://orcid.org/0000-0002-6368-1574
K Ohara https://orcid.org/0000-0002-3134-512X

References

[1] Tamura K and Inui M 2001 *J. Phys.: Condens. Matter* **13** R337
[2] Tamura K, Inui M, Matsusaka T, Ishikawa D, Kazi M H, Hong X, Isshiki M and Oh'ishi Y 2002 *J. Non-Cryst. Solids* **312–314** 269
[3] Matsuda K, Tamura K, Katoh M and Inui M 2004 *Rev. Sci. Instrum.* **75** 709
[4] Inui M, Matsuda K, Ishikawa D, Tamura K and Oh'ishi Y 2007 *Phys. Rev. Lett.* **98** 185504
[5] Hensel F and Warren W W Jr 1999 *Fluid Metals: The Liquid-Vapor Transition of Metals* (Princeton: Princeton University Press)
[6] Kajihara Y, Inui M, Matsuda K and Tamura K 2008 *J. Phys.: Conf. Ser.* **98** 012002
[7] Inui M, Matsuda K, Tamura K, Satoh K, Sobajima A and Tada H 2007 *J. Appl. Crystallogr.* **40** s537
[8] Matsuda K, Tamura K and Inui M 2007 *Phys. Rev. Lett.* **98** 096401
[9] Tamura K, Matsuda K and Inui M 2008 *J. Phys.: Condens. Matter* **20** 114102
[10] Johnson V A 1955 *Phys. Rev.* **98** 1567
[11] Kraus C A and Johnson E T 1928 *J. Phys. Chem.* **32** 1281
[12] Epstein A S 1954 *PhD Thesis* (Perdue University)
[13] Epstein A S, Fritzsche H and Lark-Horovitz K 1957 *Phys. Rev.* **107** 412
[14] Tsuchiya Y and Seymour E F W 1985 *J. Phys.* C **18** 4721
[15] Thurn H and Ruska J 1976 *J. Non-Cryst. Solids* **22** 331
[16] Tsuchiya Y 1991 *J. Phys.: Condens. Matter* **3** 3163
[17] Gitis M B and Mikhailov I G 1966 *Sov. Phys. Acoust.* **12** 14
[18] Tsuchiya Y 2002 *J. Non-Cryst. Solids* **156–158** 704
[19] Rapoport E 1968 *J. Chem. Phys.* **48** 1433
[20] Tsuchiya Y 1988 *J. Phys. Soc. Japan* **57** 3851
[21] Tsuchiya Y 1991 *J. Phys. Soc. Japan* **60** 960
[22] Hoyer W, Thomas E and Wobst M 1975 *Z. Naturforsch.* **30** 1633
[23] Bellissent R 1982 *Nucl. Instrum. Methods Phys. Res.* **199** 289
[24] Takeda S, Tamaki S and Waseda Y 1986 *J. Phys. Soc. Japan* **55** 4283
[25] Perron J C 1967 *Adv. Phys.* **16** 657
[26] Tsuchiya Y, Seymour E F W and Tsuchiya Y 1982 *J. Phys.* C **15** L687
Tsuchiya Y, Seymour E F W and Tsuchiya Y 1986 *J. Phys.* C **19** 1389
[27] Kajihara Y, Inui M, Matsuda K, Nagao T and Ohara K 2012 *Phys. Rev.* B **86** 214202
[28] Tsuchiya Y 1991 *J. Phys. Soc. Japan* **60** 227
[29] Itami T, Aoki H, Shibata T, Ikeda M and Hotozuka K 2007 *J. Non-Cryst. Solids* **353** 3011
[30] Dahlborg U, Calvo-Dahlborg U, Popel P S and Sidorov V E 2000 *Eur. Phys. J.* B **14** 639
[31] Faber T E 1972 *An Introduction to the Theory of Liquid Metals* (Cambridge: Cambridge University Press)
[32] Okada J T *et al* 2012 *Phys. Rev. Lett.* **108** 067402
[33] Matsuda K, Nagao T, Kajihara Y, Inui M, Tamura K, Nakamura J, Kimura K, Yao M, Itou M, Sakurai Y and Hiraoka N 2013 *Phys. Rev.* B **88** 115125
[34] Sastry S and Angell C A 2003 *Nat. Mater.* **2** 739
[35] Ashwin S S, Waghmare U V and Sastry S 2004 *Phys. Rev. Lett.* **92** 175701
[36] Wagner W and Pruß A 2002 *J. Phys. Chem. Ref. Data* **31** 387
[37] Rasmussen D H, MacKenzie A P, Angell C A and Tucker J C 1973 *Science* **181** 342
[38] Angell C A, Shuppert J and Tucker J C 1973 *J. Phys. Chem.* **77** 3092
[39] Poole P H, Sciortino F, Essmann U and Stanley P H 1992 *Nature* **360** 324
[40] Mishima O and Stanley H E 1998 *Nature* **396** 329
[41] Kanno H, Yokoyama H and Yoshimura Y 2001 *J. Phys. Chem.* B **105** 2019
[42] Angell C A 2007 *Nat. Nanotechnol.* **2** 396
[43] Wei S, Coleman G J, Lucas P and Angell C A 2017 *Phys. Rev. Appl.* **7** 034035
[44] Angell C A, Bressel R D, Hemmati M, Sare E J and Tucker J C 2000 *Phys. Chem. Chem. Phys.* **2** 1559
[45] Vasisht V V, Saw S and Sastry S 2011 *Nat. Phys.* **7** 549
[46] Kajihara Y, Inui M, Hosokawa S, Matsuda K and Baron A Q R 2008 *J. Phys.: Condens. Matter* **20** 494244
[47] Kajihara Y 2016 *Rev. High. Press. Sci. Technol.* **26** 288 (in Japanese)
[48] Bosio L, Teixeira J and Stanley H E 1981 *Phys. Rev. Lett.* **46** 597
[49] Xie Y, Ludwig K F Jr, Morales G, Hare D E and Sorensen C M 1993 *Phys. Rev. Lett.* **71** 2050
[50] Huang C *et al* 2009 *Proc. Natl Acad. Sci. USA* **106** 15214
Huang C *et al* 2010 *J. Chem. Phys.* **133** 134504
[51] Cunsolo A, Formisano F, Ferrero C, Bencivenga F and Finet S 2009 *J. Chem. Phys.* **131** 194502
[52] Michielsen J C F, Bot A and van der Elsken J 1988 *Phys. Rev.* A **38** 6439
[53] Clark G N I, Hura L G, Teixeira J, Soper A and Head-Gordon T 2010 *Proc. Natl Acad. Sci. USA* **107** 14003

[54] Holten V, Bertrand C E, Anisimov M A and Sengers J V 2012 *J. Chem. Phys.* **136** 094507
[55] Gallo P *et al* 2016 *Chem. Rev.* **116** 7463
[56] Kim K H, Nilsson A *et al* 2017 *Science* **358** 1589
[57] Hestand N J and Skinner J L 2018 *J. Chem. Phys.* **149** 140901
[58] Kohara S, Suzuya K, Kashihara Y, Matsumoto N, Umesaki N and Sakai I 2001 *Nucl. Instrum. Methods* **467–468** 1030
[59] Chiba A, Ohmasa Y and Yao M 2003 *J. Chem. Phys.* **119** 9047
[60] Inui M, Kajihara Y, Hosokawa S, Matsuda K, Tsuchiya Y, Tsutsui S and Baron A Q R 2019 *J. Non-Cryst. Solids* **X1** 100006
[61] Kajihara Y, Inui M and Ohara K 2016 *SPring-8/SACLA Research Reports* **4** 166
[62] Li R, Chen J, Li X, Eenge W and Limei X 2015 *New J. Phys.* **17** 063023
[63] Nishikawa K, Kouhei K, Asako Ayusawa A and Takeshi M 2003 *J. Chem. Phys.* **118** 1341
[64] Fisher M E 1964 *J. Math. Phys.* **5** 944
[65] Odagaki T, Ogita N and Matsuda H 1975 *J. Phys. Soc. Japan* **39** 618
[66] Kresse G and Hafner J 1997 *Phys. Rev.* B **55** 7539
[67] Akola J, Jones R O, Kohara S, Usuki T and Bychkov E 2010 *Phys. Rev.* B **81** 094202
[68] Barrue R and Perron J C 1985 *Phil. Mag.* B **51** 317